A&A 431, 1027–1035 (2005)
DOI: 10.1051/0004-6361:20041991

Astronomy & Astrophysics

The X-ray activity of the slowly rotating G giant δ CrB

P. Gondoin

European Space Agency, ESTEC – Postbus 299, 2200 AG Noordwijk, The Netherlands
e-mail: pgondoin@rssd.esa.int

Received 10 September 2004/ Accepted 20 October 2004

Abstract. δ CrB is a single G giant whose distinctive characteristics include an X-ray luminosity exceptionally high for a slowly rotating star. δ CrB was observed in March 2003 by the *XMM–Newton* observatory. The X-ray spectra of δ CrB are described by a MEKAL plasma model with two components at 6.5×10^6 K and 10^7 K. Series of lines of highly ionized Fe and several lines of the Ly series are visible in RGS spectra, most notably from O and Ne. The oxygen abundance is similar to the average abundance of the other elements but the Ne/O ratio found for δ CrB seems higher than in the solar photosphere, reminiscent of a similar anomaly observed in a subset of solar flares and in active stellar coronae. The spectral fitting of the EPIC and RGS spectra of δ CrB suggests a corona configuration with little contribution from quiet regions similar to the Sun. On the contrary the temperature $T \approx 6.5 \times 10^6$ K of the "cool" plasma component is reminiscent of solar type active regions, while the hot ($T \approx 10^7$ K) component may be caused by disruptions of magnetic fields associated with a permanent flaring activity. The analysis results of the *XMM–Newton* observation of δ CrB were compared with those of other single G giants with similar spectral type, mass and evolutionary status but with higher rotation rates. The comparison suggests that rapid rotation ($P < 9$ days) could increase the surface coverage with active regions and the flaring rate on G giants as expected from classical, helicity related, dynamo-driven activity. We argue that the X-ray emission of δ CrB and slowly rotating giants could be related to the existence of magnetic fields induced by turbulent motion.

Key words. stars: individual: δ CrB – stars: activity – stars: coronae – stars: evolution – stars: late-type – X-rays: stars

1. Introduction

δ CrB (HD 141714) is a chromospherically active single G giant, which shows rotational modulation of its Ca II S-index presumably due to the presence of chromospheric plages (Baliunas 1988). Choi et al. (1995) determined its rotation period from Mt Wilson Ca II H and K survey data as well as from broadband photometry to 59 days, and thus confirmed the 60.8 day period found earlier by Fernie (1987). Anticorrelations between the visual brightness and the Ca II emission support a scenario where dark spots are associated with regions of enhanced chromospheric emission (Baliunas 1988). Strassmeier (1994) found that the Ca II H and K emission lines are rather weak and determined an absolute surface flux of 8×10^5 erg cm^2 s^{-1} that shows the star to be moderately active. δ CrB shows some Li I absorption (Mallik 1999), a sign of evolutionary youth and lack of deep mixing (Wallerstein et al. 1994) consistent with its spectral type and luminosity class which indicate that the star recently became a giant. Strassmeier (1994) found a rotation velocity $v \sin i = (5 \pm 2)$ km^{-1} somewhat smaller than the earlier value $v \sin i = 8$ km^{-1} listed by Bernacca (1973) and consistent with a photometric rotation period of 59 days for a G giant. Important characteristics of δ CrB includes an X-ray luminosity greater than 10^{30} erg s^{-1} (Makarov 2003), i.e. exceptionally high for a slowly rotating giant (Gondoin 1999). I report on analysis results of X-ray spectra of δ CrB registered during an observation performed in March 2003 by the *XMM–Newton* observatory. The observations were conducted with the aim to improve our understanding of the magnetic activity on δ CrB by investigating the origin of its high X-ray luminosity and the structure of its X-ray corona.

2. δ CrB stellar parameters

A photometry study performed by Choi et al. (1995) indicates a V magnitude amplitude variation of 0.027 on δ CrB presumably due a rotational modulation by spots in the photosphere of the star. Since reliable measurements of the minimum V magnitude were not found, an upper estimate of the maximum luminosity of δ CrB was obtained by subtracting the above V amplitude variation from its $V = 4.601$ Johnson magnitude. The visual extinction of the star was neglected since δ CrB is close to the Sun and located at a high galactic latitude. The absolute magnitude was calculated from the V magnitude and from the Hipparcos parallaxes ($\pi = 19.71$ mas; ESA 1997). Alonso et al. (1999) determined an effective temperature $T_{\rm eff} = (5180 \pm 71)$ K. The luminosity of the star was estimated to 35 $L_\odot$ using the bolometric correction vs. effective temperature data of Flower (1996).

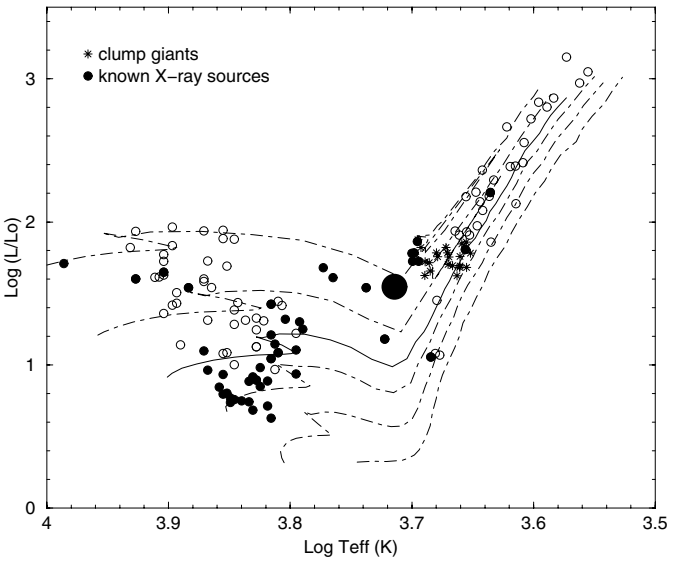

Fig. 1. $H-R$ diagram of single giants (Gondoin 1999) compared with evolutionary tracks (Schaller et al. 1992). The dot-dashed lines from bottom to top describe the evolutionary tracks of 1 $M_\odot$, 1.25 $M_\odot$, 1.5 $M_\odot$, 2 $M_\odot$ and 2.5 $M_\odot$ stars, respectively. The solid line is the evolutionary track of a 1.7 $M_\odot$ star. Open circles mark the $H-R$ diagram positions of single field giants. Black circles mark giants known as X-ray sources. The $H-R$ diagram location of δ CrB is indicated by the large spot.

Figure 1 shows the position of δ CrB in an $H-R$ diagram compared with evolutionary tracks inferred from grids of stellar models with a near solar metallicity ($Z = 0.02$) provided by Schaller et al. (1992). The models use opacities provided by Rogers & Iglesias (1991) and Kurucz (1991) and their convection parameters (i.e. mixing length ratio and overshooting parameter) have been calibrated using the red giant branch (RGB) of a wide range of clusters. The mass of δ CrB is estimated to 2.4 $M_\odot$ from its position with respect to the theoretical evolutionary tracks. The star most likely originated from an early B type, single star as it evolves in the giant domain. Li abundance measurements (Mallik 1999) support this scenario where the star has recently become a giant and is crossing the Hertzsprung gap prior the lithium depletion by convective dilution. At a later evolutionary stage when the star ascends the red giant branch, the inward expansion of its convective envelope would be expected to transport Li from the surface to the interior thus reducing its surface abundance.

The radius of δ CrB was calculated from its luminosity and effective temperature. The photometric period ($P = 59$ days; Choi et al. 1995) and the radius of the star were then used to estimate its equatorial velocity (see Table 1). Comparison with the projected rotational velocity ($v \sin i = 5 \pm 2$ km s^{-1}; Strassmeier 1994) derived spectroscopically indicates a large inclination angle of the star's polar axis onto the line of sight.

3. Observations and data reduction

δ CrB was observed by the *XMM–Newton* space observatory (Jansen et al. 2001), in revolution 591 on 2–3 March 2003

Table 1. *Top*: V magnitude, parallax and absolute magnitude of δ CrB. *Middle*: spectral type, color index and effective temperature. *Bottom*: estimated stellar parameters of δ CrB.

V	par (mas)	M_V
4.601	19.73 ± 0.73	1.05
Sp. Type	$B-V$	$T_{\rm eff}$ (K)
G3.5III	0.757	5180
R ($R_\odot$)	$v_{\rm eq}$ (km s^{-1})	M ($M_\odot$)
7.4	6.7	2.4

(see Table 2). The satellite observatory uses three grazing incidence telescopes which provide an effective area higher than 4000 cm^2 at 2 keV and 1600 cm^2 at 8 keV (Gondoin et al. 2000). One CCD EPIC pn camera (Strüder et al. 2001) and two EPIC MOS cameras (Turner et al. 2001) at the prime focus of the telescopes provide imaging in a 30 arcmin field of view and broadband spectroscopy with a resolving power of between 10 and 60 in the energy band 0.3 to 10 keV. Two identical RGS reflection grating spectrometers behind two of the three X-ray telescopes allow higher resolution ($E/\Delta E = 100$ to 500) measurements in the soft X-ray range (6 to 38 Å or 0.3 to 2.1 keV) with a maximum effective area of about 140 cm^2 at 15 Å (den Herder et al. 2001).

δ CrB observations were conducted with the EPIC pn camera operating in full frame mode (Ehle et al. 2001). RGS spectra were recorded simultaneously. "Thick" aluminium filters were used in front of the camera to reject visible light. The EPIC spectrum of δ CrB was built from photons detected within a window of 76″ diameter around the target boresight. The background was estimated on the same CCD chip as the source, within a window of the same size which was offset from the source position in an empty field region. Background rate in the EPIC camera was found to be relatively high during the first 20 ks of the observation. Due to a large increase of the background rate, the last 13 ks of the EPIC pn event list was rejected. The Pulse-Invariant (PI) spectrum was rebinned such that each resulting channel had at least 40 counts per bin. χ^2 minimization was used for spectral fitting. All fits were performed using the XSPEC package (Arnaud & Dorman 2001). The EPIC and RGS response matrices were generated by the SAS task "rmfgen" and "rgsrmfgen" respectively. The EPIC p–n spectrum was fitted in the 0.3 to 4 keV energy range. The upper cut-off of the spectral band was imposed by the decreasing count rate at high energies. The RGS spectra were analysed separately due to their higher spectral resolution in the 0.3–2.1 keV energy range.

Figure 2 shows the light curves of δ CrB obtained during revolution 591 with the p–n camera after subtraction of background events. In the 0.3–2 keV energy band, the average count rate equals 2.83 ± 0.16 s^{-1} compared with a count rate of 0.057 ± 0.026 s^{-1} in the 2–10 keV energy band. The high 0.3–2 keV over 2–10 keV count rate ratio indicates that the spectrum of δ CrB is soft. No count rate fluctuations are detected in the light curve that would suggest the

Table 2. δ CrB observation log during *XMM−Newton* revolution 591.

Experiment	Filter	Mode	Start Exp. (UT)	Exp. Duration
p−n	Thick	Full Frame	2 March 2003 @ 04:35:38	30 046 s
RGS1		Spec + Q	2 March 2003 @ 04:36:33	33 685 s
RGS2		Spec + Q	2 March 2003 @ 04:36:33	33 685 s

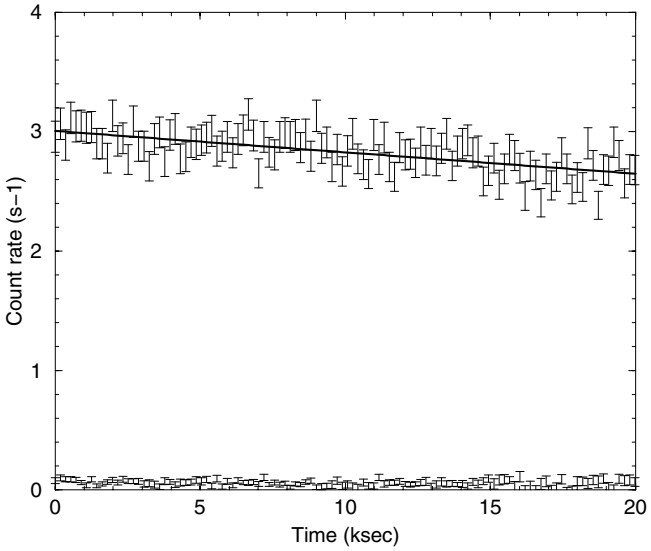

Fig. 2. X-ray light curves of δ CrB obtained with the EPIC p−n camera during *XMM−Newton* revolution 591. The upper curve is the count rate within the 0.3 to 2 keV band and the lower curve is the count rate within the 2 to 10 keV band. The events are binned in 180 s time intervals and the background contribution has been subtracted.

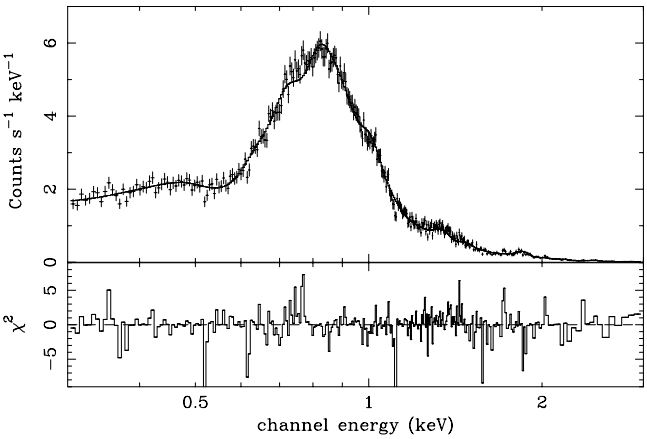

Fig. 3. Best fit model to the EPIC pn spectrum of δ CrB. The EPIC data (crosses) and spectral fit (solid line) are shown in the upper panel and the χ^2 contributions in the lower panel.

Table 3. Best fit parameters to EPIC data using a 2 components MEKAL model (Mewe et al. 1985). The spectral fitting was conducted in the 0.3–4 keV band with the same abundance relative to the Sun for the two temperature components.

Model parameter	Best fit value
$N_{\rm H}$ (10^{20} cm^{-2})	6.5 ± 0.5
Z	0.19 ± 0.01
kT_1 (keV)	0.56 ± 0.02
EM_1 (10^{52} cm^{-3})	34 ± 5
kT_2 (keV)	0.86 ± 0.09
EM_2 (10^{52} cm^{-3})	15 ± 8
χ^2	1.27 (395/311 d.o.f.)

presence of flares. The count rate in the low energy band decreased steadily by ≈12% in 20 ks. Spectral fitting of the EPIC data (see Sect. 5.1) yields flux measurements in the 0.3−2 keV and >2 keV bands. These measurements were converted into X-ray luminosities $L_{0.3-2\ \rm keV} = 37.2 \times 10^{29}$ erg s^{-1} and $L_{>2\ \rm keV} = 1.4 \times 10^{29}$ erg s^{-1} using Hipparcos parallax (π = 19.73 mas; ESA 1997). The hardness ratio $hr = -0.93$ defined as $hr = (L_{>2\ \rm keV} - L_{0.3-2\ \rm keV})/(L_{>2\ \rm keV} + L_{0.3-2\ \rm keV})$ confirms that the X-ray spectrum of δ CrB is soft.

4. Spectral analysis

4.1. Analysis of EPIC data

The EPIC dataset (see Fig. 3) was fitted with the MEKAL optically thin plasma emission model (Mewe et al. 1985). The spectral fitting was performed in the 0.3–4 keV spectral band. The interstellar hydrogen column density was left free to vary. A value $N_{\rm H} = (6.5 \pm 0.5) \times 10^{20}$ cm^{-2} was derived which is comparable to the total galactic H I column density in the direction of δ CrB (Dickey & Lockman 1990). No single temperature plasma model that assumes either solar photospheric (Anders & Grevesse 1989) or non-solar abundances can fit the data, as unacceptably large values of χ^2 are obtained. A MEKAL plasma model with two components at different temperatures proves acceptable. The addition of a third component to the model does not improve the quality of the spectral fit.

The best fit temperatures of the plasma components are 6.5×10^6 K and 10^7 K respectively. The average element abundance in the δ CrB corona is found to be lower than the solar photospheric value (see Table 3). Among all of the different changes, eruption and instabilities seen on the Sun, the ones labeled "flares" all have in common material heated to temperatures of 10^7 K or higher (Golub & Pasachoff 1997; Reale et al. 2001). Such temperatures are not seen in the non-flaring corona, and events which do not produce such hot plasma do not seem to be called flares. In active stellar coronae, it has been proposed that the peak in emission measure around 10^7 K is due to flaring activity (Drake et al. 2000;

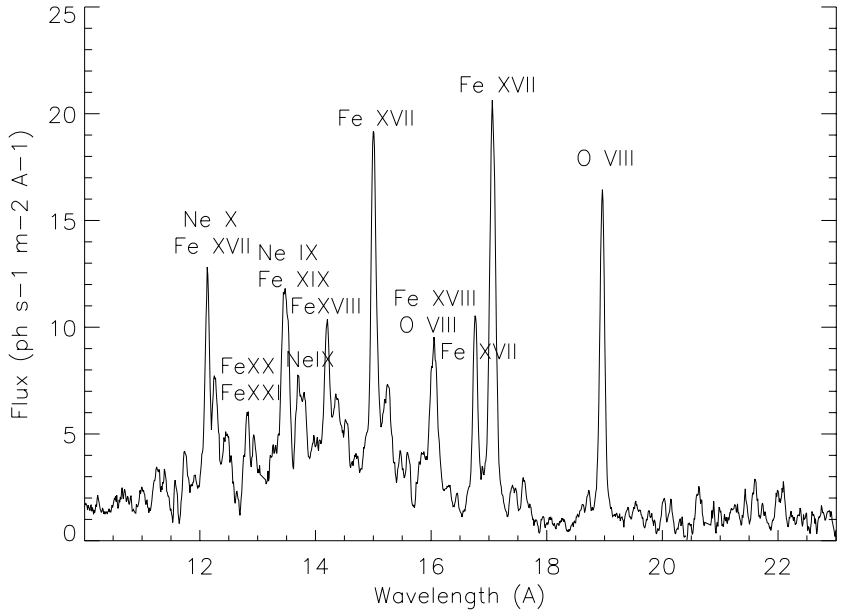

Fig. 4. RGS spectrum of δ CrB in the 10 Å−23 Å band.

Sanz-Forcada et al. 2002). However, such a flaring activity is expected to induce count rate fluctuations that are not observed in the EPIC light curves of δ CrB. Hence, although suggestive, the existence of significant amounts of 10^7 K material cannot be regarded as proof of the presence of flares in the corona of δ CrB.

4.2. Analysis of RGS data

Figure 4 shows the RGS spectrum of δ CrB obtained after a 33 ks exposure. The spectrum is the sum of the two spectra simultaneously obtained with the RGS1 and RGS2 reflection grating spectrometers on board *XMM−Newton*. Line fluxes and positions were measured using the XSPEC package by fitting simultaneously the RGS1 and RGS2 spectra with a sum of narrow Gaussian emission lines convolved with the response matrices of the RGS instruments. The continuum emission was described using Bremstrahlung models at the temperatures of the plasma components inferred from the analysis of EPIC data. For line identification, we required only that the wavelength coincidence be comparable to the spectral resolution of the RGS spectrometers, namely 0.04 Å over the 5 to 35 Å wavelength range. In the X-ray domain, several candidate lines may exist within this acceptable wavelength coincidence range. Series of lines of highly ionized Fe and several lines of the Ly series are visible in RGS spectra, most notably from O and Ne. Table 5 lists the measurements of lines that are statistically significant and gives the line fluxes corrected for interstellar absorption ($N_{\rm H} = 6.5 \times 10^{20}$ cm^{-2}) on the line of sight to δ CrB. Their temperatures of maximum formation range between 3×10^6 K and 1.6×10^7 K indicating that the corresponding ions are associated with the plasma component inferred from EPIC data. Lines such as the O VIII and Ne X lines have emissivity functions quite spread in temperature. The flux measurement of some lines such as Ne X (12.13 Å) is affected by blends.

Electron densities can be measured using density sensitive spectral lines originating from metastable levels, such as the forbidden (f) 2^3S-1^1S line in helium-like ions. This line and the associated resonance (r) 2^1P-1^1S and intercombination (i) 2^3P-1^1S lines make up the so-called helium like triplet lines (Gabriel & Jordan 1969; Pradhan 1982; Mewe et al. 1985). The intensity ratio $G = (i + f)/r$ varies with electron temperature and the ratio $R = f/i$ varies with electron density due to the collisional coupling between the metastable 2^3S upper level of the forbidden line and the 2^3P upper level of the intercombination line. The RGS wavelength band contains the He-like triplets from O VII, Ne IX, Mg XI and Si XIII. However, the Si and Mg triplets are not sufficiently resolved, the Ne IX triplet is too heavily blended with iron lines for unambiguous density analysis and the helium-like O VII triplet is barely detected in the X-ray spectrum of δ CrB (see Fig. 4).

The low energy RGS spectra were fitted with a VMEKAL model with two components at different temperatures. The VMEKAL model generates a spectrum of hot diffuse gas with line emission from several elements based on the calculation of Mewe et al. (1985) with Fe-L shell calculations by Liedahl (1995). Hence, two electron temperatures and electron densities are assumed for the entire ensemble of element charge states and in particular for iron, oxygen and neon which produce the most prominent lines. This assumption turns out to be fairly adequate within the observational uncertainties of the present spectrum (see Fig. 4). The fit was performed in the spectral range from 10 Å to 25 Å where the efficiency of the RGS spectrometers is the highest. The model temperatures of the plasma components were frozen to the values derived from EPIC data (see Table 3). The abundances of the O and Ne elements which give prominent lines in the considered spectral range were first tied to the abundance of the other elements (MODEL A). They were then allowed to vary independently but with the same value for all temperature

Table 4. Best fit parameters to RGS spectra in the 0.5−1.3 keV range using a two components VMEKAL model. The temperature of each component were frozen to the value derived from the analysis of EPIC data (see Table 3). The metallicity was left free to vary. The oxygen and neon abundances were first tied to the abundance of the other elements (MODEL A). There were then left free to vary independently but with the same value for the different temperature components (MODEL B).

Parameter	MODEL A	MODEL B
kT_1 (keV)	0.56	0.56
EM_1 (10^{52} cm^{-3})	27 ± 2	28 ± 2
kT_2 (keV)	0.86	0.86
EM_2 (10^{52} cm^{-3})	15 ± 2	14 ± 2
O	0.17	0.17 ± 0.02
Ne	0.17	0.26 ± 0.03
Other abundances	0.17 ± 0.01	0.16 ± 0.01
χ^2	1.24	1.23
	1490/1206 d.o.f.	1477/1204 d.o.f.

components (MODEL B). Fitting results are given in Table 4. The fit supports the two components plasma model for the interpretation of the EPIC and RGS data. The emission measures of the two temperature components are similar to the values derived from the analysis of EPIC spectra (see Table 3). When left free to vary, the oxygen abundance is similar to the average abundance of the other elements. The determination of abundances relative to hydrogen requires an accurate measurement of the X-ray continuum which cannot be reliably measured even from the RGS spectra (see Fig. 4) due to their moderate spectral resolution and signal to noise ratio. Therefore it is modeled from the flux left over when all of the known emission lines in the VMEKAL model are included. However, no plasma spectroscopy code includes all of the emission lines, so the missing weak emission lines are misinterpreted as continuum flux (Schmitt et al. 1996), thereby raising the hydrogen abundance derived from the free-free continuum and lowering all of the metal abundances relative to hydrogen. This systematic error in the metal abundances relative to hydrogen is not included in the abundance uncertainties stated in Table 4 but the fitting results suggest that neon abundance of the hot plasma component is significantly higher than the oxygen abundance. The improvement in χ^2 fit statistics ($\Delta\chi^2/\Delta\nu = 13$ for 1202 degrees of freedom) induced with variable O and Ne abundance is significant at >99% confidence using the F-statistic. Hence, the Ne/O ratio found for δ CrB seems higher than in the solar photosphere. This indication of a Ne abundance enhancement is reminiscent of a similar anomaly observed in a subset of solar flares (Murphy et al. 1991; Schmelz 1993). Large Ne abundance enhancements are a common feature of active stellar coronae (Güdel et al. 2001; Huenemoerder et al. 2001) and an inverse FIP effect is observed in very active coronae (Brinkman et al. 2001; Drake et al. 2001) where the abundances (relative to oxygen) increase with increasing first ionization potential (FIP).

5. Discussion

One striking peculiarity of δ CrB is its X-ray luminosity that is exceptionally high for a slowly rotating giant. In order to investigate the origin of this high X-ray luminosity, the analysis results of the *XMM−Newton* observation of δ Cr B were compared with those of other single G giants with similar spectral type, mass and evolutionary status but with higher rotation rates. The sample of comparison giants include V1794 Cygni (Gondoin 2004), HR 9024 (Gondoin 2003a), V390 Aurigae (Gondoin 2003b) and FK Comae (Gondoin 2002). These single stars are classified as FK Comae type stars due to their rapid rotation. They are single giants with fast rotating A or B type progenitors on the main sequence. As δ CrB, they are evolving near the bottom of the red giant branch. Their stellar parameters and X-ray luminosities in the 0.3−2 keV and >2 keV bands are summarized in Table 6. With the exception of the most massive star HR 9024, a correlation seems to exist among the sample giants between X-ray luminosity and rotation rate. The X-ray luminosity dependance with rotation is higher in the high energy band. The ratio between the luminosity of δ Crb, the slowest rotator, and that of FK Comae, the fastest spinning star, is one order of magnitude in the low energy band and two order of magnitude or more in the high energy band.

The spectral fitting of the EPIC and RGS spectra of δ CrB suggests a corona configuration with little contribution from quiet regions similar to the Sun. On the contrary the temperature $T \approx 6.5 \times 10^6$ K of the "cool" plasma component is reminiscent of solar type active regions, while the hot ($T \approx 10^7$ K) component may be caused by disruptions of magnetic fields associated to a permanent flaring activity. The review of coronal activity by Vaiana & Rosner (1978) pointed out that the Sun, if completely covered with active regions, would have an X-ray luminosity of 2×10^{29} erg s^{-1}. When scaled to the surface of δ CrB ($R \approx 7.4\ R_\odot$; see Table 1), an X-ray luminosity of about 110×10^{29} erg s^{-1} is obtained. The X-ray luminosity (27×10^{29} erg s^{-1}) of the "cool" plasma component ($T \approx 6.5 \times 10^6$ K) can be explained if about 24% of δ CrB surface is covered with solar-like active regions. Assuming that these active regions are described by a simple system of similar loops with constant pressure p (dyn cm^{-2}), temperature T (K) and cross section A (cm^2), the emission measure EM (cm^{-3}) of the "cool" plasma can be expressed as:

$$EM = GF \times (4\pi R^2) \times \left(\frac{p}{2kT}\right)^2 \times L \quad (1)$$

where R is the stellar radius, F is the filling factor and L the loop half-length. G is a geometry factor which includes effect of partial occultation of the corona by the star itself (i.e. G varies from 0.5 to 1 for $L \ll R$ to $L \gg R$). Using the relation $T = 1400 \times (pL)^{1/3}$ (Rosner et al. 1978) and $G = 0.7$, a characteristic loop length scale is obtained (Mewe et al. 1982):

$$L_{10} = 7.4F \times T_7^4 \times EM_{52}^{-1} \times (R/R_\odot)^2 \quad (2)$$

where L_{10} is the loop half length in units of 10^{10} cm, T_7 is the coronal temperature in unit of 10^7 K, and EM_{52} is the emission

Table 5. Positions, transition, temperatures of maximum line formation and fluxes of the strongest lines in RGS spectra.

λ_{meas} (Å)	λ_{pred} (Å)	Ion	Transition	log (T_{max}) log (K)	$F_{meas.}$ (10^{-6} cm^{-2} s^{-1})
12.13	12.13	Ne X	$2p^2P_{1/2,3/2}-1s^2S_{1/2}$	6.8	195 ± 32
	12.12	Fe XVII	$2s^22p^5(^2P)4d^3D_1-2s^22p^6\ ^1S_0$	6.8	
	12.16	Fe XXIII	$1s^22s3s^1S_0-1s^22s2p^1P_1$	7.2	
12.82	12.82	Fe XX	$1s^22s^22p^{1/2}2p^{3/2}3d^{3/2}-2s^22p^3\ ^4S_{3/2}$	7.0	81 ± 26
	12.82	Fe XXI	$1s^22s2p^{1/2}2p^{3/2}3d^{5/2}-1s^22s2p^3\ ^3D_1$	7.0	
	12.85	Fe XX	$1s^22s^22p^{1/2}2p^{3/2}3d^{3/2}-2s^22p^3\ ^4S_{3/2}$	7.0	
	12.86	Fe XX	$1s^22s^22p^{1/2}2p^{3/2}3d^{5/2}-2s^22p^3\ ^4S_{3/2}$	7.0	
13.45	13.45	Ne IX	$1s2p^1P_1-1s^2\ ^1S_0$	6.6	222 ± 33
	13.46	Fe XIX	$2s^22p^3(^2D)3d^3S_1-2s^22p^4\ ^3P_2$	6.9	
13.70	13.70	Ne IX	$1s2s^3S_1-1s^2\ ^1S_0$	6.6	125 ± 27
14.20	14.21	Fe XVIII	$1s^22s^22p^{1/2}2p^3_{3/2}3d^{5/2}-2s^22p^5\ ^2P_{3/2}$	6.9	224 ± 24
	14.21	Fe XVIII	$2s^22p^4(^1D)3d^2D_{5/2}-2s^22p^5\ ^2P_{3/2}$	6.9	
15.01	15.01	Fe XVII	$2s^22p^5(^2P)3d^1P_1-2s^22p^6\ ^1S_0$	6.7	365 ± 28
16.00	16.00	O VIII	$3p^2P_{1/2,3/2}-1s^2S_{1/2}$	6.5	173 ± 23
	16.00	Fe XVIII	$2s^22p^4(^3P)3s^2P_{3/2}-2s^22p^5\ ^2P_{3/2}$	6.8	
16.80	16.77	Fe XVII	$2s^22p^5(^2P)3s^1P_1-2s^22p^6\ ^1S_0$	6.7	154 ± 25
18.96	18.97	O VIII	$2p^2P_{1/2}-1s^2S_{1/2}$	6.5	154 ± 29
	18.97	O VIII	$2p^2P_{3/2}-1s^2S_{1/2}$	6.5	

Table 6. Spectral type, effective temperature, radius, mass and rotational period of δ CrB and comparison giants with higher rotation rates.

	Sp. Type	T_{eff} (K) (K)	R ($R_\odot$) ($R_\odot$)	M ($M_\odot$) ($M_\odot$)	P (days) (days)	$L_{0.3-2\ keV}$ (10^{30} erg s^{-1})	$L_{>2\ keV}$ (10^{30} erg s^{-1})
δ CrB	$G_{3.5}$ III	5180	7.4	2.4	59	3.7	0.14
HR 9024	G_1 III	5110	10–13	2.8–3.1	23	22–27	10–73
V390 Aur	G_8 III	4970	6.7	1.8	9.8	3.9–5.3	3.0–6.1
V1794 Cyg	G_5 III	5450	4.6–5.5	1.7–1.9	3.3	14–21	5–14
FK Com	G_5 III	5080	5.9–9.9	2.0–2.7	2.4	18–46	12–55

measure in units of 10^{52} cm^{-3}. Inserting the observed temperature and emission measure of the cool plasma component (see Table 3) and $R = 7.4\ R_\odot$ (see Table 1), we find $L \approx 5 \times 10^9$ cm assuming a ≈24% filling factor. The pressure scale height H (in cm) is given by $H = 5 \times 10^3 \times T \times (g/g_\odot)^{-1}$ where $g/g_\odot$ is the surface gravity expressed in solar units and T the temperature in Kelvin. For δ CrB, $g/g_\odot = 0.44$ using $M = 2.4\ M_\odot$ and $R = 7.4\ R_\odot$ (see Table 1). Since it turns out that the loop lengths are much smaller than the pressure scale height H, the assumption of constant pressure in the loops is justified. The characteristic loop size and temperature on δ CrB are respectively 5×10^9 cm and 6.5×10^6 K.

The characteristic surface coverage, active region emission measures, loop temperatures, sizes and densities were derived previously for the comparison giants using a similar analysis procedure (Gondoin 2002, 2003a,b, 2004). The results are summarized in Table 7 and suggest that the effect of rotation on giants is to increase their surface coverage with solar-like active regions. This coverage would be a factor 2 to 3 higher for fast (<4 days) rotating giants compared to slow (>9 days) rotating giants. The static loop model gives characteristic loop size, temperature and densities of (5–30) × 10^9 cm, (6.5–8.5) × 10^6 K, and (0.6–2) × 10^{10} cm^{-3} respectively. Solar corona observations by comparison show bright hot loops within active regions which reach maximum temperatures and electron densities above the neutral line of typically (3–4) × 10^6 K and 10^{10} cm^{-3} (Vaiana et al. 1973). In addition to these hot loops, on-disk images of the Sun show that neighboring active regions are often connected into complexes of activity by large loop-like structures (Van Speybroek et al. 1970). Such

Table 7. Active region coverage and parameters of a simple coronal loop model for δ CrB and comparison giants with higher rotation rates.

	P (days)	Coverage (%)	T (10^6 K)	EM (10^{52} cm^{-3})	L (10^9 cm)	n_e (10^{10} cm^{-3})
δ CrB	59	24	6.5	34	5	2
HR 9024	23	15–31	7.5–7.7	62–72	9–12	1.3–1.7
V390 Aur	9.8	25–30	7.2	19	13	1.1
V1794 Cyg	3.3	55–88	7.9–8.1	35–43	13–14	1.2–1.3
FK Com	2.4	30–50	8.5	41	30	0.6

Table 8. Flare indicators for δ CrB and comparison giants with high rotation rates.

	P (days)	Variability	$EM_{T>10^7\ K}$ (10^{52} cm^{-3})	T_{Max} (10^6 K)	Fe K line (at ≈6.7 keV) EW (eV)	[O]/[Fe]	[Ne]/[Fe]
δ CrB	59	No	14–15	10	No	1.0	1.6
HR 9024	23	No	250–299	42–43	400	1.0	3.5
V390 Aur	9.8	No	20–39	13–14	No	1.0	2.3
V1794 Cyg	3.3	No	155–254	75–85	400	2.1	8.0–9.1
FK Com	2.4	Yes	182–585	38–62	411–723	1.2	4.4

interconnecting loops can be longer than 10^{10} cm, but tend to be cooler than loops within solar active regions and therefore cooler than coronal loops on G giants.

In contrast to the marked difference between fast (<4 days) and slowly (>9 days) rotating giants, the surface coverage with active regions would be relatively similar for the slowly rotating stars V390 Aur, HR 9024 and δ CrB. In spite of their slow rotation, the X-ray luminosity of these stars would be as if 25% of their surfaces were covered with solar-like active region. Gilliland (1985) indicated that slow rotation leads to a large Rossby number, and hence reduces classical, helicity related, dynamo-driven activity. This suggests that a parameter other than rotation plays an important role in determining the level of X-ray activity on slowly rotating giants. Rosner et al. (1995) remarked that the absence of a large-scale dynamo does not imply the suppression of magnetic field production, driven by the turbulent motion in the convection zones. They suggest rather that a large-scale organized surface magnetic flux emergence normally associated with stellar activity disappears on slowly rotating stars, and is replaced by magnetic flux emergence arising from a seed field placed in a turbulent convection zone. Closed structures can remain if their spatial scale falls below the atmosphere's pressure scale height (Antiochos et al. 1986) which is in the range $(500-1700) \times 10^9$ cm for (1.7−3.1) $M_\odot$ giants. Hence, the X-ray emission on δ CrB and slowly rotating giants could be related to magnetic fields produced by turbulent motions.

If, in δ CrB, the cool plasma component is produced by corona loops covering a significant fraction of the star's surface, it is easy to imagine that these closed structures interact and that the disruption of their magnetic fields which might be expected then leads to flaring. Table 8 lists flare indicators that were derived from the analysis of X-ray spectra of δ CrB and of the comparison giants. Flare indicators include light curve variability, the emission measure and maximum temperature of hot (>10^7 K) plasma, the presence of an Fe K-shell line around 6.7 keV indicative of the presence of iron in high states of ionization, and an enhancement of the oxygen and neon abundance relative to iron. FK Comae excepted, no significant variability has been detected in the light curve of the sample stars. This can be interpreted as an absence of large flares during their observations. However, if a large fraction of their surface is covered by active regions and coronal loops, flares could be so frequent that their light curves overlap, canceling out any variability due to single events. Frequent flares would explain the important emission measure of hot plasma above 10^7 K on δ CrB and on the comparison giants. High temperature (>10^7 K) plasmas have been detected from the Sun and from non-solar coronae (van den Oord & Mewe 1989; Tsuru et al. 1989; Antonucci & Dodero 1995; Griffiths & Jordan 1998; Sanz-Forcada et al. 2002). This aspect is much debated and still open, but it has been suggested that this hot component may be due to a continuous flaring activity (Güdel 1997; Drake et al. 2000). This could explain the presence of hot material in the corona of δ CrB and other active G giants (Gondoin 2003a,b, 2004) even in the absence of obvious flares. There could be small-scale flares not well identified in the light curves with moderate signal to noise ratio. The flatness of the δ CrB's light curve (see Fig. 2) could be explained if the heating of its corona results from a large number of small flares. Recent studies of the flaring rates in magnetically active stars as a function of flare energy indicate power-law distributions that may be sufficient to explain all coronal radiative losses (Audard et al. 2000; Kashyap et al. 2002; Güdel et al. 2003). It is worth

noting that, with the exception of the massive giant HR 9024, the emission measure and temperature of hot plasma seem to increase with the rotation rate (see Table 8). This supports the idea that the flaring rate on giants could increase with the stellar rotation rate. This statement is corroborated by the fact that iron in high ionization states and large Ne abundance enhancements are detected in the fast rotating giants V1794 Cygni and FK Comae and not in the slowly rotating giants V390 Aurigae and δ CrB. It is worth noting that the massive giants HR 9024 presents signs of intense flaring in spite of its low rotation suggesting that a parameter other than rotation play a crucial role in determining the level of X-ray emission of slowly rotating giants.

6. Summary

δ CrB is a single G giant whose distinctive characteristics include an X-ray luminosity exceptionally high for a slowly rotating star. δ CrB was observed in March 2003 by the *XMM−Newton* observatory. The high 0.3−2 keV over 2−10 keV count rate ratio indicates that the spectrum of δ CrB is soft. No count rate fluctuations are detected in the light curve that would suggest the presence of large flares. The EPIC spectrum of δ CrB is described by a MEKAL plasma model with two components at 6.5×10^6 K and 10^7 K. Series of lines of highly ionized Fe and several lines of the Ly series are visible in RGS spectra, most notably from O and Ne. Their temperatures of maximum formation range between 3×10^6 K and 1.6×10^7 K. The oxygen abundance is similar to the average abundance of the other elements but the Ne/O ratio found for δ CrB seems higher than in the solar photosphere, reminiscent of a similar anomaly observed in a subset of solar flares and in active stellar coronae. The spectral fitting of the EPIC and RGS spectra of δ CrB suggests a coronal configuration with little contribution from quiet regions similar to the Sun. On the contrary the temperature $T \approx 6.5 \times 10^6$ K of the "cool" plasma component is reminiscent of solar type active regions, while the hot ($T \approx 10^7$ K) component may be caused by disruptions of magnetic fields associated with a permanent flaring activity. The analysis results of the *XMM−Newton* observation of δ Cr B were compared with those of other single G giants with similar spectral type, mass and evolutionary status but with different rotation rates. The comparison suggests that rapid rotation ($P < 9$ days) on G giants could increase their surface coverage with solar-like active regions as expected from classical, helicity related, dynamo-driven activity. The comparison also suggests that the flaring rate on giants increases with the stellar rotation rate. Confirmation of these trends requires the X-ray observation of a large sample of G giants with similar evolutionary status. We argue that the X-ray emission from δ CrB and slowly rotating giants could be related to magnetic fields produced by turbulent motion.

Acknowledgements. I thank my colleagues from the *XMM−Newton* Science Operation Center for their support in implementing the observations. I am grateful to the referee, Dr. Paterno, for the helpful comments.

References

Anders, E., & Grevesse, N. 1989, Geochim. Cosmochim. Acta, 53, 197
Antiochos, S. K., Haisch, B. M., & Stern, R. A. 1986, ApJ, 307, L55
Antonucci, E., & Dodero, M. A. 1995, ApJ, 438, 480
Arnaud, K., & Dorman, B. 2001, XSPEC User's Guide for version 11.1, http://heasarc.gsfc.nasa.gov/docs/xanadu/xspec/manual/manual.html
Audard, M., Güdel, M., Drake, J. J., et al. 2000, ApJ, 541, 396
Baliunas, S. L. 1988, in Automatic Small Telescopes, ed. D. S. Hayes, & R. M. Genet (Fairborn Press, Mesa), 83
Baliunas, S. L. 1988, in Solar Radiative Output Variation, ed. P. Foukal (Cambridge: Cambridge Research and instrumentation), 230
Bernacca, P. L. 1973, Contr. Oss. Astr. Univ. Padova Asiago, No. 294
Brinkman, A. C., Behar, E., Güdel, M., et al. 2001, A&A, 365, L324
Choi, H. J., Soo, W., Donahue, R. A., et al. 1995, PASP, 107, 744
Dickey, J. M., & Lockman, F. J. 1990, ARA&A, 28, 215
den Herder, J. W., Brinkman, A. C., Kahn, S. M., et al. 2001, A&A, 365, L7
Drake, J. J., Peres, G., Orlando, S., et al. 2000, ApJ, 545, 1074
Drake, N. A., Brickhouse, N. S., Kashyap, V., et al. 2001, ApJ, 548, L81
Ehle, M., Breitfellner, M., Dahlem, M., et al. 2001, The XMM−Newton Users' Handbook, http://xmm.vilspa.esa.es/user/A02/uhb/xmm_uhb.html
ESA 1997, The Hipparcos Catalogue, ESA SP-1200
Fernie, J. D. 1987, PASP, 99, 183
Flower, P. J. 1996, ApJ, 469, 335
Gabriel, A. H., & Jordan, C. 1969, MNRAS, 145, 241
Gilliland, R. L. 1985, ApJ, 299, 286
Golub, L., & Pasachoff, J. M. 1997, in The Solar Corona (Cambridge, UK: Cambridge University Press)
Gondoin, P. 1999, A&A, 352, 217
Gondoin, P. 2003a, A&A, 404, 355
Gondoin, P. 2003b, A&A, 409, 263
Gondoin, P. 2004, A&A, 413, 1095
Gondoin, P., Aschenbach, B., Erd, C., et al. 2000, SPIE Proc., 4140, 1
Gondoin, P., Erd, C., & Lumb, D. 2002, A&A, 383, 919
Griffiths, N. W., & Jordan, C. 1998, ApJ, 497, 1998
Güdel, M. 1997, ApJ, 480, L121
Güdel, M., Audard, M., Briggs, K., et al. 2001, A&A, 365, L336
Güdel, M., Audard, M., Smith, K. W., et al. 2003, in 12th Cambridge Workshop on Cool Stars, Stellar Systems, and the Sun (2001 July 30−August 3), ed. A. Brown, G. M. Harper, & T. R. Ayres (University of Colorado), 303
Huenemoerder, D. P., Canizares, C. R., & Schulz, N. S. 2001, ApJ, 559, 1135
Jansen, F., Lumb, D., Altieri, B., et al. 2001, A&A, 365, L1
Kashyap, V. L., Drake, J. J., Güdel, M., et al. 2002, ApJ, 580, 1118
Kurucz, R. L. 1991, in Stellar Atmospheres: Beyond Classical Models, NATO ASI Series C, Vol. 341
Liedahl, D. A., Osterheld, A. L., & Goldstein, W. H. 1995, ApJ, 438, 115
Mallik, S. W. 1999, A&A, 352, 495
Makarov, V. V. 2003, AJ, 126, 1996
Mewe, R., Gronenschild, E. H. B. M., Heise, J., et al. 1982, ApJ, 260, 233
Mewe, R., Gronenschild, E. H. B., & van den Oord, G. H. J. 1985, A&A, 62, 197
Murphy, R. J., Ramaty, R., Reames, D. V., et al. 1991, ApJ, 371, 793
Pradhan, A. K. 1982, ApJ, 263, 477
Reale, F., Peres, G., & Orlando, S. 2001, ApJ, 557, 906
Rogers, F. J., & Iglesias, C. A. 1992, ApJS, 79, 507

Rosner, R., Tucker, W. H., & Vaiana, G. S. 1978, ApJ, 220, 643
Rosner, R., Musielak, Z. E., Cattaneo, F., et al. 1995, ApJ, 442, L25
Sanz-Forcada, J., Brickhouse, N. S., & Dupree, A. K. 2002, ApJ, 570, 799
Schaller, G., Schaerer, D., Meynet, G., et al. 1992, A&AS, 96, 269
Schmelz, J. T. 1993, ApJ, 408, 373
Schmitt, J. H. M. M., Drake, J. J., & Stern, R. A. 1996, ApJ, L465, 51
Strassmeier, K. G., Handler, G., Paunzen, E., et al. 1994, A&A, 281, 855
Strüder, L., Briel, U., Dennerl, K., et al. 2001, A&A, 365, L18
Tsuru, T., Makishima, K., Ohashi, T., et al. 1989, PASJ, 41, 679
Turner, M. J. L. T., Abbey, A., Arnaud, M., et al. 2001, A&A, 365, L27
Vaiana, G. S., Davis, J. M., Giacconi, R., et al. 1973, ApJ, 185, 47
Vaiana, G. S., & Rosner, R. 1978, ARA&A, 16, 393
van den Oordt, G. H. J., & Mewe, R. 1989, A&A, 213, 245
Van Speybroeck, L. P., Krieger, A. S., & Vaiana, G. S. 1970, Nature, 227, 818
Wallerstein, G., Bohm-Vitense, E., Vanture, A. D., & Gonzales, G. 1994, AJ, 107, 2211